Applied Catalysis B: Environmental 181 (2016) 570–580

Contents lists available at ScienceDirect

Applied Catalysis B: Environmental

journal homepage: www.elsevier.com/locate/apcatb

MnO_x supported on Fe–Ti spinel: A novel Mn based low temperature SCR catalyst with a high N_2 selectivity

Shijian Yang[a,b,*], Feihong Qi[a], Shangchao Xiong[a], Hao Dang[a], Yong Liao[a], Po Keung Wong[b,**], Junhua Li[c,***]

[a] Jiangsu Key Laboratory of Chemical Pollution Control and Resources Reuse, School of Environmental and Biological Engineering, Nanjing University of Science and Technology, Nanjing 210094, PR China
[b] School of Life Sciences, The Chinese University of Hong Kong, Shatin, NT, Hong Kong SAR, PR China
[c] State Key Joint Laboratory of Environment Simulation and Pollution Control (SKLESPC), School of Environment, Tsinghua University, Beijing 100084, PR China

ARTICLE INFO

Article history:
Received 9 February 2015
Received in revised form 25 June 2015
Accepted 11 August 2015
Available online 15 August 2015

Keywords:
10% Mn/Fe–Ti spinel
N_2O selectivity
Reaction mechanism
Steady state kinetic study
Transient reaction

ABSTRACT

In this work, a novel 10% Mn/Fe–Ti spinel catalyst with an excellent N_2 selectivity was developed for the selective catalytic reduction (SCR) of NO with NH_3 at low temperatures. The mechanism of NO reduction and N_2O formation over Fe–Ti spinel, 10% Mn/Fe–Ti spinel and 5% Mn–10% Fe/TiO_2 was investigated using in situ DRIFT study and the transient reaction study. Meanwhile, the reaction kinetic constant of the SCR reaction (i.e., N_2 formation) through the Eley–Rideal mechanism, the reaction kinetic constant of the SCR reaction through the Langmuir–Hinshelwood mechanism and the reaction kinetic constant of the non selective catalytic reduction (NSCR) reaction (i.e., N_2O formation) were obtained according to the steady state kinetic study. They all indicate that the NSCR reaction over 10% Mn/Fe–Ti spinel through the Eley–Rideal mechanism was cut off. NH_2 adsorbed on 10% Mn/Fe–Ti spinel can be hardly oxidized to NH as NH_2 mainly adsorbed on the support (i.e., Fe–Ti spinel) of 10% Mn/Fe–Ti spinel, which was far away from Mn^{4+} cations on 10% Mn/Fe–Ti spinel. Therefore, the NSCR reaction over 10% Mn/Fe–Ti spinel through the Eley–Rideal mechanism was suppressed. However, the regeneration of Fe^{3+} on Fe–Ti spinel was accelerated due to the rapid electron transfer between Mn^{4+} and Fe^{2+} on 10% Mn/Fe–Ti spinel resulting in a remarkable promotion on NH_3 activation although NH_3 adsorbed on 10% Mn/Fe–Ti spinel cannot be directly activated by Mn^{4+} on 10% Mn/Fe–Ti spinel. Therefore, the SCR reaction over Fe–Ti spinel was promoted remarkably after the load of MnO_x. As a result, 10% Mn/Fe–Ti spinel showed an excellent SCR performance especially N_2 selectivity at low temperatures, which was much better than 5% Mn-10% Fe/TiO_2 with the same chemical composition.

1. Introduction

The most cost-effective method to control NO_x emission from coal-fired power plants is the selective catalytic reduction (SCR) of NO with NH_3 [1]. Nowadays, V_2O_5-WO_3(MoO_3)/TiO_2 is widely used as the commercial SCR catalysts [2], which is located upstream of the electrostatic precipitator (ESP) due to its narrow operating temperature window of 300–400 °C [3]. Because the space and access upstream of the electrostatic precipitator are limited, it is very difficult to retrofit the SCR units in many existing power plants [4]. Therefore, the low temperature SCR catalysts, which are placed downstream of the electrostatic precipitator and desulfurizer, are strongly demanded [5]. Mn based SCR catalysts, for example Mn/TiO_2 [6,7], Mn–Fe/TiO_2 [8], MnO_x-CeO_2 [9,10], MnO_x-CeO_2/TiO_2 [11,12], Mn promoted V_2O_5/TiO_2 [13] and Mn–Fe spinel [14], show an excellent SCR activity at low temperatures. However, Mn based catalysts are extremely restricted in the low temperature SCR reaction for at least two reasons: the lower N_2 selectivity and the deactivation by SO_2 [5,15]. Firstly, the non selective catalytic reduction (NSCR) reaction can simultaneously happen during the SCR reaction over Mn based SCR catalysts [1], resulting in the formation of a lot of N_2O. As N_2O contributes to global warming and stratospheric ozone depletion, it has been considered as a pollu-

* Corresponding author at: Jiangsu Key Laboratory of Chemical Pollution Control and Resources Reuse, School of Environmental and Biological Engineering, Nanjing University of Science and Technology, Nanjing, 210094, PR China.
** Corresponding author.
*** Corresponding author.
E-mail addresses: yangshijiangsq@163.com (S. Yang), pkwong@cuhk.edu.hk (P.K. Wong), lijunhua@tsinghua.edu.cn (J. Li).

http://dx.doi.org/10.1016/j.apcatb.2015.08.023
0926-3373/

tant [16–18]. Secondly, there still is a small amount of SO_2 in the flue gas downstream of the flue gas desulphurization (FGD), which often lead to an unrecoverable deactivation on the low temperature SCR reaction over Mn based SCR catalyst [10].

There is generally agreement that both the Eley–Rideal mechanism and the Langmuir–Hinshelwood mechanism could contribute to N_2O formation over Mn based SCR catalyst and N_2O formation over Mn based SCR catalyst mainly resulted from the Eley–Rideal mechanism especially at higher temperatures [19]. Therefore, the most effective way to restrain N_2O formation over Mn based catalyst is to cut off the route of N_2O formation through the Eley–Rideal mechanism (i.e., suppress the over-activation of NH_2 to NH by Mn^{4+} on the surface). In this work, a novel Mn based low temperature SCR catalyst (i.e., Mn/Fe–Ti spinel) with an excellent N_2 selectivity was devised. NH_2 adsorbed on Mn/Fe–Ti spinel cannot be oxidized to NH as NH_2 mainly adsorbed on the support (i.e., Fe–Ti spinel) of Mn/Fe–Ti spinel, which was far away from Mn^{4+} cations on Mn/Fe–Ti spinel. Meanwhile, the regeneration of Fe^{3+} on Fe–Ti spinel was accelerated due to the rapid electron transfer between Mn^{4+} and Fe^{2+} on Mn/Fe–Ti spinel resulting in a remarkable promotion on NH_3 activation although NH_3 adsorbed cannot be directly activated by Mn^{4+} on Mn/Fe–Ti spinel. Therefore, Mn/Fe–Ti spinel showed an excellent SCR performance (including the SCR activity and N_2 selectivity) at low temperatures. Especially, N_2 selectivity of NO reduction over Mn/Fe–Ti spinel was much better than those over other Mn based SCR catalysts.

2. Experimental

2.1. Catalyst preparation

Fe–Ti spinel was prepared using a co-precipitation method followed by the thermal treatment under air for 3 h at 500 °C [20,21]. 10% Mn/Fe–Ti spinel was prepared by the conventional impregnation method using manganese nitrate as precursor and Fe–Ti spinel as support. The sample was dried at 105 °C overnight after the removal of excess water by a rotary evaporator, and then calcined at 500 °C for 3 h under air. Meanwhile, 5%Mn–10%Fe/TiO_2 was prepared as a comparison by the conventional impregnation method using manganese nitrate and ferric nitrate as precursors and Degussa TiO_2 P25 as support [8].

2.2. Catalytic test

The catalytic reaction was performed on a fixed-bed quartz tube reactor and the internal diameter of the reactor was 6 mm. The gas hourly space velocity (GHSV) was 2.4×10^4 cm^3 g^{-1} h^{-1} (i.e., the mass of catalyst with 40–60 mesh was 500 mg, and the total flow rate was 200 mL min^{-1}). The typical reactant gas contained 500 ppm of NO (when used), 500 ppm of NH_3 (when used), 60 ppm of SO_2 (when used), 2% of O_2, 8% of H_2O (when used) and balance of N_2. An infrared spectrometer (Thermo SCIENTIFIC, ANTARIS, IGS Analyzer) was used to determine the concentrations of NO, NO_2, NH_3, and N_2O online.

Meanwhile, the steady state kinetic study was performed. The catalyst mass was 5–100 mg, the total flow rate was 200 mL min^{-1}, and the corresponding GHSV was 120000–2400000 cm^3 g^{-1} h^{-1}, resulting in a less than 15% of NO_x conversion to overcome the diffusion limitation (including the inner diffusion and external diffusion). Gaseous NO concentration in the inlet varied from 200 to 500 ppm, while gaseous NH_3 concentration was kept at 500 ppm.

Furthermore, the transient reaction at 150 °C was performed. The catalyst mass was 100 mg, the total flow rate was 200 mL min^{-1}, and the corresponding GHSV was 120000 cm^3 g^{-1} h^{-1}. Prior to each experiment, the catalyst was heated at 300 °C in a flow of N_2 (200 mL min^{-1}) for 60 min to remove adsorbed H_2O and other gases. The catalyst was first treated by 500 ppm of NO and 2% of O_2 for 30 min followed by N_2 purged for 10 min. 500 ppm of NH_3 was then introduced. Then, the reactants were introduced to the catalyst in the reversed order. The concentrations of N_2O, NH_3, NO and NO_2 in the outlet during the transient reaction were determined online. Meanwhile, in situ DRIFT spectra during the transient reaction were collected 32 scans with a resolution of 4 cm^{-1} using another infrared spectrometer (Nicolet NEXUS 870).

2.3. Catalyst characterization

A nitrogen adsorption apparatus (Quantachrome, Autosorb-1) was used to determine the BET surface. X-ray diffraction patterns (XRD) were recorded on an X-ray diffractionmeter (Bruker-AXS D8 Advance). A chemisorption analyzer (Micromeritics, ChemiSorb 2720 TPx) was used to record the H_2-temperature programmed reduction (H_2-TPR) profile. Temperature programmed desorption of ammonia (NH_3-TPD) and that of NO (NO-TPD) were both carried out on the packed-bed quartz tube reactor. A X-ray photoelectron spectroscopy (Thermo fisher K-Alpha) was used to determine the Fe 2p, Ti 2p, Mn 2p and O 1s binding energies on Fe-Ti spinel, 10% Mn/Fe–Ti spinel and 5% Mn–10% Fe/TiO_2.

3. Results

3.1. SCR performance

3.1.1. SCR activity

Fig. 1a shows that NO reduction over Fe–Ti spinel was remarkably promoted after the load of MnO_x. NO_x conversion over 10% Mn/Fe–Ti spinel was close to that of 5% Mn–10% Fe/TiO_2 below 150 °C and was much higher than that of 5% Mn–10% Fe/TiO_2 above 175 °C. Although a small amount of N_2O formed over Fe–Ti spinel after the load of MnO_x (shown in Fig. 1b), N_2O selectivity of NO reduction over 10% Mn/Fe–Ti spinel was generally lower than 8%, which was much less than that over 5% Mn–10% Fe/TiO_2 (shown in Fig. 1c). As a result, the amount of N_2 formed during NO reduction over 10% Mn/Fe–Ti spinel was much higher than that over 5% Mn–10% Fe/TiO_2 (shown in Fig. 1d). They suggest that the SCR performance of 10% Mn/Fe–Ti spinel was much better than that of 5% Mn–10% Fe/TiO_2 although they have the same chemical composition.

3.1.2. Effect of H_2O and SO_2

Then, the effect of 8% of H_2O and 60 ppm of SO_2 on NO reduction over 10% Mn/Fe–Ti spinel was investigated. As shown in Fig. 2a, the presence of H_2O showed a notable deactivation on NO reduction below 200 °C. Meanwhile, the deactivation was remarkably enhanced after the further introduction of SO_2. However, NO reduction over 10% Mn/Fe–Ti spinel was hardly affected by the presence of SO_2 and H_2O above 200 °C (shown in Fig. 2a). Fig. 2b shows the stability of NO reduction over 10% Mn/Fe–Ti spinel at 200 °C in the presence of 8% of H_2O and 60 ppm of SO_2. After the introduction of H_2O and SO_2, NO_x conversion at 200 °C gradually decreased and it was kept at approximately 83%. Meanwhile, the formation of a small amount of N_2O over 10% Mn/Fe–Ti spinel was completely suppressed in the presence of H_2O and SO_2. After the removal of H_2O and SO_2, NO_x conversion over 10% Mn/Fe–Ti spinel rapidly recovered to 100%. They suggest that 10% Mn/Fe–Ti spinel showed an excellent H_2O and SO_2 durability above 200 °C for the SCR reaction.

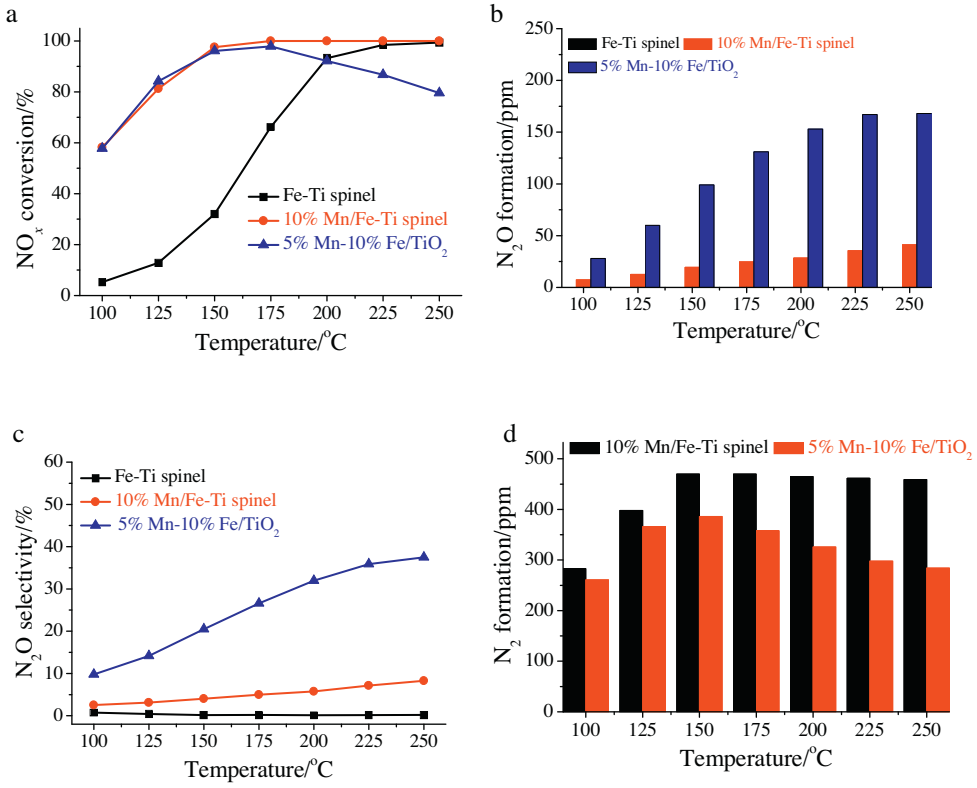

Fig. 1. SCR performance of Fe–Ti spinel, 10% Mn/Fe–Ti spinel and 5% Mn-10% Fe/TiO_2: (a), NO_x conversion; (b), N_2O formation; (c), N_2O selectivity; (d), N_2 formation. Reaction conditions: [NH_3] = [NO] = 500 ppm, [O_2] = 2%, catalyst mass = 500 mg, total flow rate = 200 mL min^{-1} and GHSV = 24000 cm^3 g^{-1} h^{-1}.

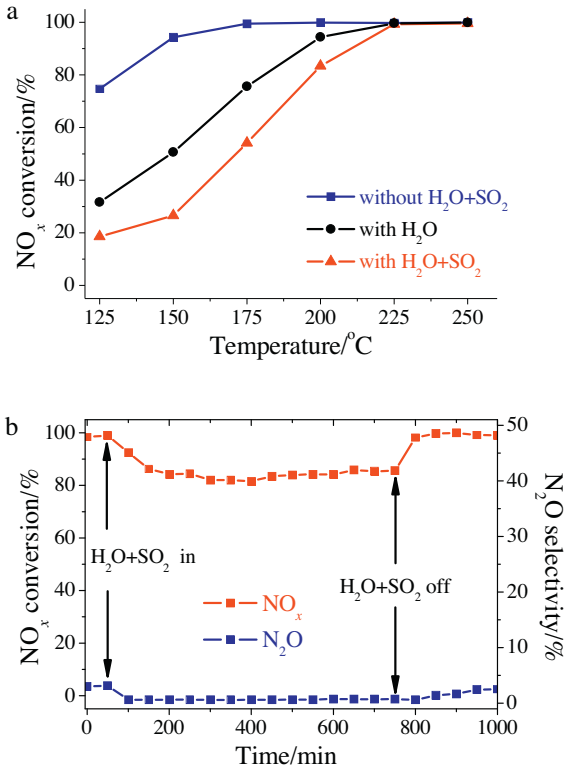

Fig. 2. (a), Effect of H_2O and SO_2 on the low temperature SCR reaction over 10% Mn/Fe–Ti spinel. (b), Stability of NO reduction over 10% Mn/Fe–Ti spinel in the presence of H_2O and SO_2. Reaction conditions: [NH_3] = [NO] = 500 ppm, [SO_2] = 60 ppm, [H_2O] = 8%, catalyst mass = 500 mg, the total flow rate = 100 mL and GHSV = 12000 cm^3 g^{-1} h^{-1}.

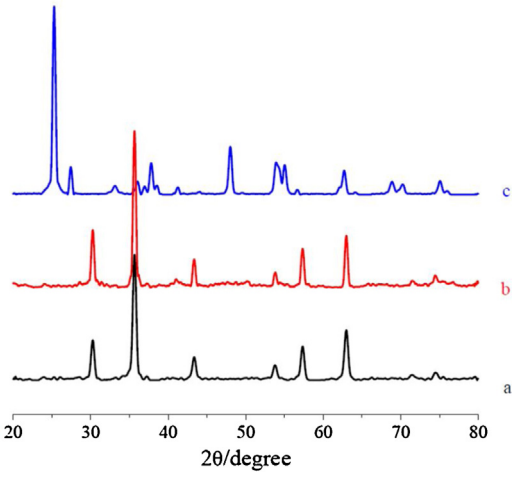

Fig. 3. XRD patterns of: (a), Fe–Ti spinel; (b), 10% Mn/Fe–Ti spinel; (c), 5% Mn–10% Fe/TiO_2.

3.2. Catalytic characterization

3.2.1. XRD and BET

XRD patterns of Fe–Ti spinel, 10% Mn/Fe–Ti spinel and 5% Mn–10% Fe/TiO_2 were shown in Fig. 3. The characteristic peaks of Fe–Ti spinel corresponded very well to the standard card of maghemite (JCPDS: 39-1346) [20]. After the loading of MnO_x, no additional characteristic reflections corresponding to crystalline manganese oxides appeared (shown in Fig. 3). It suggests that MnO_x was well dispersed on Fe–Ti spinel. As P25 contains both rutile and anatase [3], the reflections of anatase (JCPDS: 21-1272) and rutile (JCPDS: 21-1276) both appeared in the XRD pattern of 5% Mn–10%

Table 1
The ratio of Ti, Mn, Fe and O species on Fe–Ti spinel, 10% Mn/Fe–Ti spinel and 5% Mn–10% Fe/TiO_2 /%.

	Fe^{3+}	Ti^{4+}	O^{2-}	Mn		
				Mn^{2+}	Mn^{3+}	Mn^{4+}
Fe–Ti spinel	25.5	12.1	62.4	–	–	–
10% Mn/Fe–Ti spinel	20.2	12.5	62.9	0.6	1.4	2.4
5% Mn–10% Fe/TiO_2	3.3	28.5	65.7	0.7	0.8	1.0

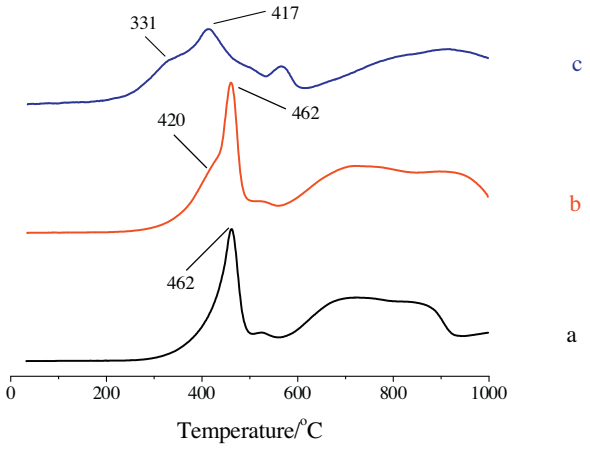

Fig. 4. H_2-TPR profiles of: (a), Fe–Ti spinel; (b), 10% Mn/Fe–Ti spinel; (c), 5% Mn–10% Fe/TiO_2.

Fe/TiO_2. However, additional reflections that would indicate the presence of other crystalline iron oxides and manganese oxides cannot be observed in the diffraction scan. It suggests that both MnO_x and FeO_x in 5% Mn–10% Fe/TiO_2 were well dispersed on P25.

The BET surface area of Fe–Ti spinel, 10% Mn/Fe–Ti spinel and 5% Mn–10% Fe/TiO_2 were 108, 61.8 and 40.9 $m^2\,g^{-1}$ respectively.

3.2.2. XPS

The ratios of Fe, Ti, O and Mn species on Fe–Ti spinel, 10% Mn/Fe–Ti spinel and 5% Mn–10% Fe/TiO_2 can be collected from XPS spectra (shown in Fig. S1 in the Supporting materials). As shown in Table 1, the ratio of Fe^{3+} on Fe–Ti spinel obviously decreased after the load of MnO_x. It suggests that MnO_x probably preferred to cover Fe^{3+} than Ti^{4+} on Fe-Ti spinel. Furthermore, Table 1 shows that the percent of Mn^{4+} on 10% Mn/Fe–Ti spinel was much higher than that on 5% Mn–10% Fe/TiO_2.

3.2.3. TPR

TPR profile recorded from Fe–Ti spinel showed two obvious reduction peaks. The peak centered at about 462 °C was assigned to the reduction of $(Fe_2Ti)_{0.8}O_4$ to Fe_2TiO_4, and the broad peak at higher temperature was attributed to the reduction of Fe_2TiO_4 to Fe [21]. After the load of MnO_x, a new peak appeared at 420 °C (shown in Fig. 4), which was related to the reduction of loaded MnO_x. TPR profile of 5% Mn–10% Fe/TiO_2 showed four obvious reduction peaks. The peak at 331 °C was assigned to the reduction of highly dispersed MnO_x [22], the peak at 417 °C was probably assigned to the reduction of Fe_2O_3 and Mn_3O_4 [22], and the reduction peaks above 500 °C was probably attributed to the reduction of FeO to Fe [20]. Fig. 4 suggests that the oxidation ability of synthetic catalyst increased as the following sequence: Fe–Ti spinel<10% Mn/Fe–Ti spinel<5% Mn–10% Fe/TiO_2.

3.2.4. NH_3 adsorption and NO adsorption

The capacities of Fe–Ti spinel, 10% Mn/Fe–Ti spinel and 5% Mn–10% Fe/TiO_2 for NH_3 and NO adsorption can be calculated from

Table 2
Capacities of Fe–Ti spinel, 10% Mn/Fe–Ti spinel and 5% Mn–10% Fe/TiO_2 for NO and NH_3 adsorption at 50 °C/μmol m^{-2}.

	NH_3	NO
Fe–Ti spinel	3.0	0.51
10% Mn/Fe–Ti spinel	3.2	1.2
5% Mn–10% Fe/TiO_2	3.9	2.1

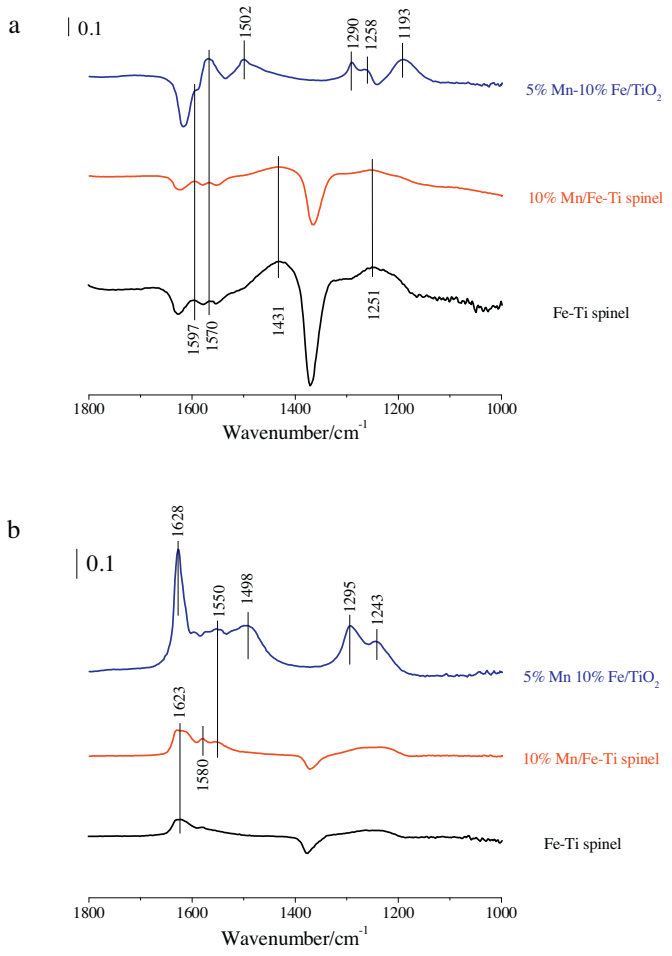

Fig. 5. (a), In situ DRIFT spectra of the adsorption of NH_3 at 150 °C over Fe–Ti spinel, 10% Mn/Fe–Ti spinel and 5% Mn–10% Fe/TiO_2; (b), In situ DRIFT spectra of the adsorption of NO + O_2 at 150 °C over Fe–Ti spinel, 10% Mn/Fe–Ti spinel and 5% Mn–10% Fe/TiO_2.

NH_3-TPD and NO-TPD profiles (show in Fig. S2 in the Supporting materials). As shown in Table 2, the capacity of Fe–Ti spinel for NH_3 adsorption did not vary notably after the load of MnO_x. However, the capacity of Fe–Ti spinel for NO + O_2 adsorption obviously increased after the load of MnO_x. They suggest that the acidity of Fe–Ti spinel was not affected remarkably after the load of MnO_x, while the adsorption of NO on Fe–Ti spinel was remarkably promoted. Table 2 also shows that the capacities of 5% Mn–10% Fe/TiO_2 for NH_3 and NO adsorption were both much more than those of Fe–Ti spinel and 10% Mn/Fe–Ti spinel.

Fig. 5 shows in situ DRIFT spectra of the adsorption of NH_3 and NO + O_2 on Fe–Ti spinel, 10% Mn/Fe–Ti spinel and 5% Mn–10% Fe/TiO_2 at 150 °C. After the adsorption of NH_3 over Fe–Ti spinel, four characteristic vibrations at 1597, 1570, 1431, and 1251 cm^{-1} appeared. The band at 1597 cm^{-1} was assigned to coordinated NH_3 bound to the Lewis acid sites, the band at 1431 cm^{-1} was attributed to ionic NH_4^+ bound to the Brønsted acid sites, and the bands at 1570 and 1251 cm^{-1} could be related to the oxidation/deformation

of adsorbed NH_3 [21]. In situ DRIFT spectra of the adsorption of NH_3 over 10% Mn/Fe–Ti spinel was the same as that over Fe–Ti spinel (shown in Fig. 5a). It suggests that the acidity of Fe–Ti spinel did not vary after the load of MnO_x and the acid sites on 10% Mn/Fe–Ti spinel mainly resulted from the support (i.e., Fe–Ti spinel). After the adsorption of NH_3 over 5% Mn–10% Fe/TiO_2, six characteristic vibrations at 1597, 1570, 1502, 1290, 1258, and 1193 cm^{-1} appeared, which was quite different from those over Fe–Ti spinel and 10% Mn/Fe–Ti spinel. The bands at 1597 and 1193 cm^{-1} were assigned to coordinated NH_3 bound to the Lewis acid sites and the bands at 1570, 1502, 1290, and 1258 cm^{-1} were attributed to the oxidation/deformation of adsorbed NH_3 [23,24].

After the adsorption of NO + O_2 over Fe–Ti spinel at 150 °C, only a characteristic vibration at 1623 cm^{-1} can be clearly observed (shown in Fig. 5b), which was assigned to monodentate nitrite [21,25]. However, three characteristic vibrations at 1623, 1580, and 1550 cm^{-1} appeared after the adsorption of NO + O_2 over 10% Mn/Fe–Ti spinel at 150 °C. The bands at 1623 and 1550 cm^{-1} were assigned to mondentate nitrite, and the band at 1580 cm^{-1} was assigned to monodentate nitrate [24,25]. After the adsorption of NO + O_2 on 5% Mn–10% Fe/TiO_2 at 150 °C, five characteristic vibrations at 1628, 1550, 1498, 1295, and 1243 cm^{-1} appeared. The bands at 1628, 1550, and 1243 cm^{-1} were assigned to monodentate nitrite, and the bands at 1498 and 1295 cm^{-1} was attributed to monodentate nitrate [4,24,25].

3.3. Transient reaction

3.3.1. 5% Mn–10% Fe/TiO_2

After the adsorption of NO + O_2 at 150 °C, 5% Mn–10% Fe/TiO_2 was mainly covered by monodentate nitrite (at 1628, 1550, and 1243 cm^{-1}) and monodentate nitrate (at 1498 and 1295 cm^{-1}) (shown in Fig. 6a). After the further introduction of NH_3, these bands corresponding to adsorbed NO_x gradually diminished, and 5% Mn–10% Fe/TiO_2 was at last covered by coordinated NH_3 (at 1597 and 1193 cm^{-1}) and the oxidation/deformation species of adsorbed NH_3 (at 1570, 1502, 1290, and 1258 cm^{-1}). It suggests that the Langmuir–Hinshelwood mechanism (i.e., the reaction of adsorbed NO_x with adsorbed NH_3) contributed to NO reduction over 5% Mn–10% Fe/TiO_2. Fig. 7a shows that a small amount of N_2O formed during the introduction of NH_3 to NO + O_2 pretreated 5% Mn–10% Fe/TiO_2. There is generally agreement that the product of the reaction between nitrite and adsorbed NH_3 was N_2, while that of the reaction between nitrate and adsorbed NH_3 was N_2O [1]. They suggest that the Langmuir–Hinshelwood mechanism (i.e., the reaction of adsorbed monodentate nitrate with adsorbed NH_3) contributed to N_2O formation during NO reduction over 5% Mn–10% Fe/TiO_2.

After the adsorption of NH_3 at 150 °C, 5% Mn–10% Fe/TiO_2 was mainly covered by coordinated NH_3 (at 1597 and 1193 cm^{-1}) and the oxidation/deformation species of adsorbed NH_3 (at 1570, 1502, 1290, and 1258 cm^{-1}). These bands corresponding to adsorbed NH_3 species all rapidly diminished after the further introduction of NO + O_2 (shown in Fig. 6b). It suggests that the Eley–Rideal mechanism (i.e., the reaction of adsorbed NH_3 species with gaseous NO) contributed to NO reduction over 5% Mn–10% Fe/TiO_2. Fig. 7b shows that N_2O concentration in the outlet rapidly increased to 13 ppm and then gradually diminished during the introduction of NO + O_2 to NH_3 pretreated 5% Mn–10% Fe/TiO_2. It suggests that the Eley–Rideal mechanism (i.e., the reaction of over-activated NH_3 with gaseous NO) contributed to N_2O formation during NO reduction over 5% Mn–10% Fe/TiO_2. Fig. 7 shows that the amount of N_2O formed during the introduction of NO + O_2 to NH_3 pretreated 5% Mn–10% Fe/TiO_2 was much higher than that formed during the introduction of NH_3 to NO + O_2 pretreated 5% Mn–10% Fe/TiO_2. It suggests that N_2O formation during NO reduction over 5% Mn–10% Fe/TiO_2 mainly resulted from the Eley–Rideal mechanism.

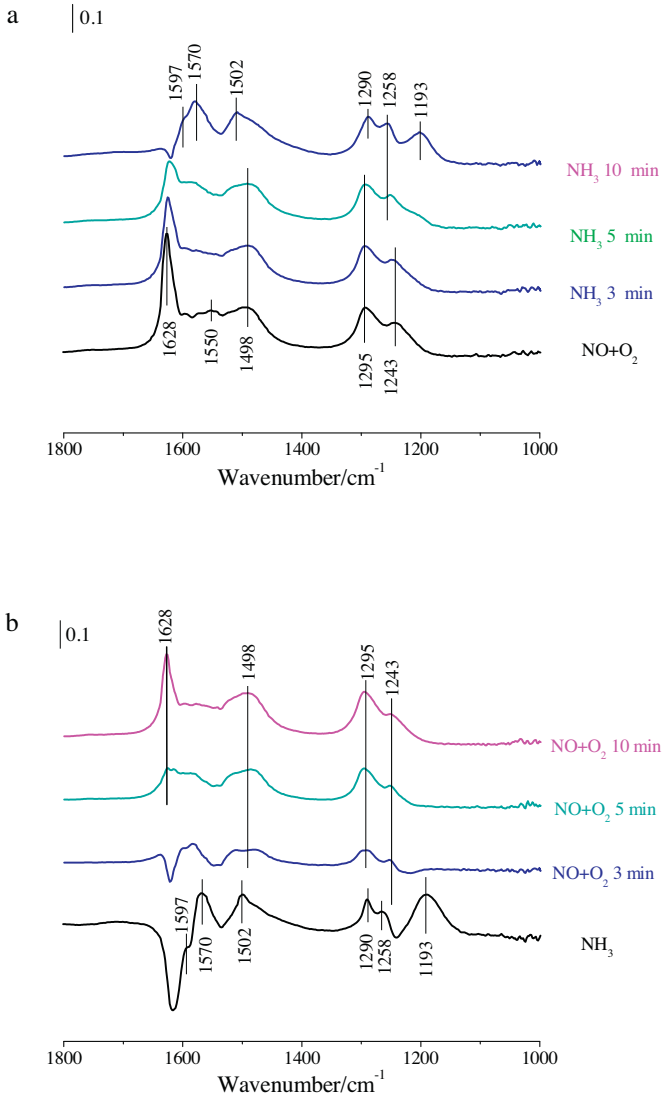

Fig. 6. (a), In situ DRIFT spectra taken at 150 °C upon passing NH_3 over NO + O_2 presorbed 5% Mn–10% Fe/TiO_2; (b), In situ DRIFT spectra taken at 150 °C upon passing NO + O_2 over NH_3 presorbed 5% Mn–10% Fe/TiO_2.

3.3.2. Fe–Ti spinel

After the adsorption of NO + O_2 at 150 °C, Fe–Ti spinel was mainly covered by monodentate nitrite (at 1623 cm^{-1}). After the further introduction of NH_3, monodentate nitrite on Fe–Ti spinel rapidly diminished and Fe–Ti spinel was at last covered by coordinated NH_3 (at 1597 cm^{-1}), ionic NH_4^+ (at 1431 cm^{-1}) and the oxidation/deformation species of adsorbed NH_3 (at 1570 and 1251 cm^{-1}) (shown in Fig. 8a). It suggests that the Langmuir–Hinshelwood mechanism contributed to NO reduction over Fe–Ti spinel.

After the adsorption of NH_3 at 150 °C, Fe–Ti spinel was mainly covered by coordinated NH_3 (at 1597 cm^{-1}), ionic NH_4^+ (at 1431 cm^{-1}) and the oxidation/deformation species of adsorbed NH_3 (at 1570 and 1251 cm^{-1}). After the further introduction of NO + O_2, these bands corresponding to adsorbed NH_3 species gradually diminished and Fe–Ti spinel was at last covered by monodentate nitrite (at 1623 cm^{-1}). It suggests that the Eley–Rideal mechanism also contributed to NO reduction over Fe–Ti spinel.

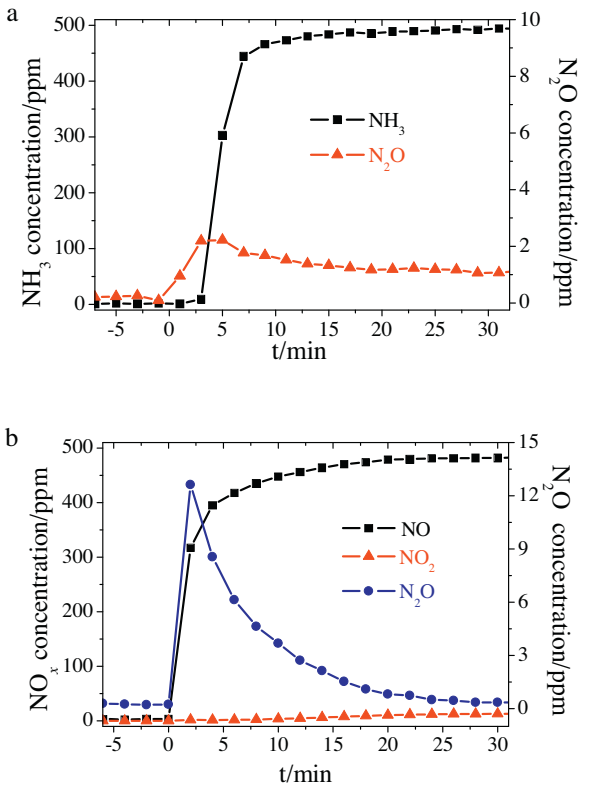

Fig. 7. (a), NH_3 and N_2O concentrations in the outlet during passing NH_3 over $NO + O_2$ presorbed 5% Mn–10% Fe/TiO_2 at 150 °C; (b), NO_x and N_2O concentrations in the outlet during passing $NO + O_2$ over NH_3 presorbed 5% Mn–10% Fe/TiO_2 at 150 °C.

3.3.3. 10% Mn/Fe–Ti spinel

After the adsorption of $NO + O_2$ at 150 °C, 10% Mn/Fe–Ti spinel was mainly covered by monodentate nitrite (at 1623 and 1550 cm^{-1}) and monodentate nitrate (at 1580 cm^{-1}). After the further introduction of NH_3, these bands corresponding to adsorbed NO_x gradually diminished, and 10% Mn/Fe–Ti spinel was at last covered by coordinated NH_3 (at 1597 cm^{-1}), ionic NH_4^+ (at 1431 cm^{-1}) and the oxidation/deformation species of adsorbed NH_3 (at 1570 and 1251 cm^{-1}) (shown in Fig. 9a). It suggests that the Langmuir–Hinshelwood mechanism contributed to NO reduction over 10% Mn/Fe–Ti spinel. Fig. 10a shows that a small amount of N_2O formed during the introduction of NH_3 to $NO + O_2$ pretreated 10% Mn/Fe–Ti spinel, which mainly resulted from the reaction between adsorbed monodentate nitrate and adsorbed NH_3 (i.e., the Langmuir–Hinshelwood mechanism).

After the adsorption of NH_3 at 150 °C, 10% Mn/Fe–Ti spinel was mainly covered by coordinated NH_3 (at 1597 cm^{-1}), ionic NH_4^+ (at 1431 cm^{-1}) and the oxidation/deformation species of adsorbed NH_3 (at 1570 and 1251 cm^{-1}), which was the same as Fe–Ti spinel. After the further introduction of $NO + O_2$, these bands corresponding to adsorbed NH_3 species gradually diminished and 10%Mn/Fe–Ti spinel was at last covered by monodentate nitrite (at 1623 and 1550 cm^{-1}) and monodentate nitrate (at 1580 cm^{-1}) (shown in Fig. 9b). It suggests that the Eley–Rideal mechanism contributed to NO reduction over 10%Mn/Fe–Ti spinel. However, only a small amount of N_2O formed during the introduction of $NO + O_2$ to NH_3 pretreated 10% Mn/Fe–Ti spinel (shown in Fig. 10b), which was much less than that formed during the introduction of $NO + O_2$ to NH_3 pretreated 5% Mn–10%Fe/TiO_2 (shown in Fig. 8b). Meanwhile, the amount of N_2O formed during the introduction of NH_3 to $NO + O_2$ pretreated 10% Mn/Fe–Ti spinel (shown in Fig. 10a) was close to that formed during the introduction of NH_3 to $NO + O_2$ pre-

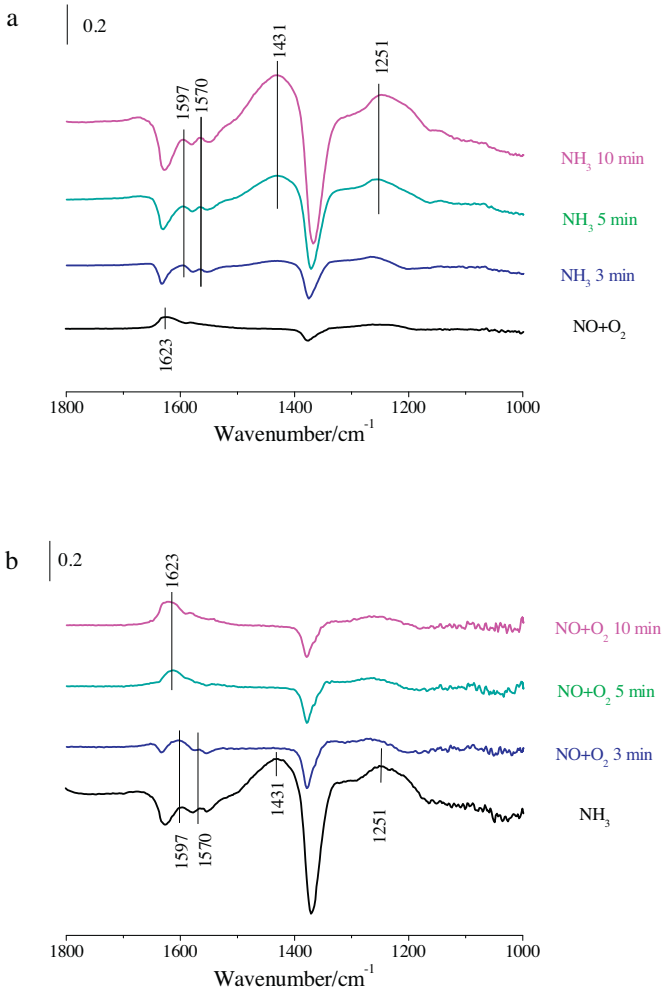

Fig. 8. (a), In situ DRIFT spectra taken at 150 °C upon passing NH_3 over $NO + O_2$ presorbed Fe–Ti spinel; (b), In situ DRIFT spectra taken at 150 °C upon passing $NO + O_2$ over NH_3 presorbed Fe-Ti spinel.

treated 5% Mn–10% Fe/TiO_2 (shown in Fig. 7a). They suggest that the lower N_2O selectivity of NO reduction over 10%Mn/Fe–Ti spinel as compared with 5% Mn–10%Fe/TiO_2 was mainly related to the suppression of N_2O formation through the Eley–Rideal mechanism.

4. Discussion

4.1. Reaction mechanism

In situ DRIFT study demonstrates that both the Eley–Rideal mechanism and the Langmuir–Hinshelwood mechanism contributed to NO reduction over Fe–Ti spinel, 10% Mn/Fe–Ti spinel and 5% Mn–10% Fe/TiO_2. Meanwhile, the transient reaction study demonstrates that both the Eley–Rideal mechanism and the Langmuir–Hinshelwood mechanism contributed to N_2O formation over 10% Mn/Fe–Ti spinel and 5% Mn–10% Fe/TiO_2.

NO reduction through the Langmuir–Hinshelwood mechanism can be approximately described as [1,15,23,26,27]:

$$NH_{3(g)} \rightarrow NH_{3(ad)} \quad (1)$$

$$NO_{(g)} \rightarrow NO_{(ad)} \quad (2)$$

$$M^{n+} = O + NO_{(ad)} \rightarrow Mn^{(n-1)+}\text{- O- NO} \quad (3)$$

$$M^{n+} = O + NO_{(g)} + \frac{1}{2}O_2 \rightarrow M^{(n-1)+}\text{- O- } NO_2 \quad (4)$$

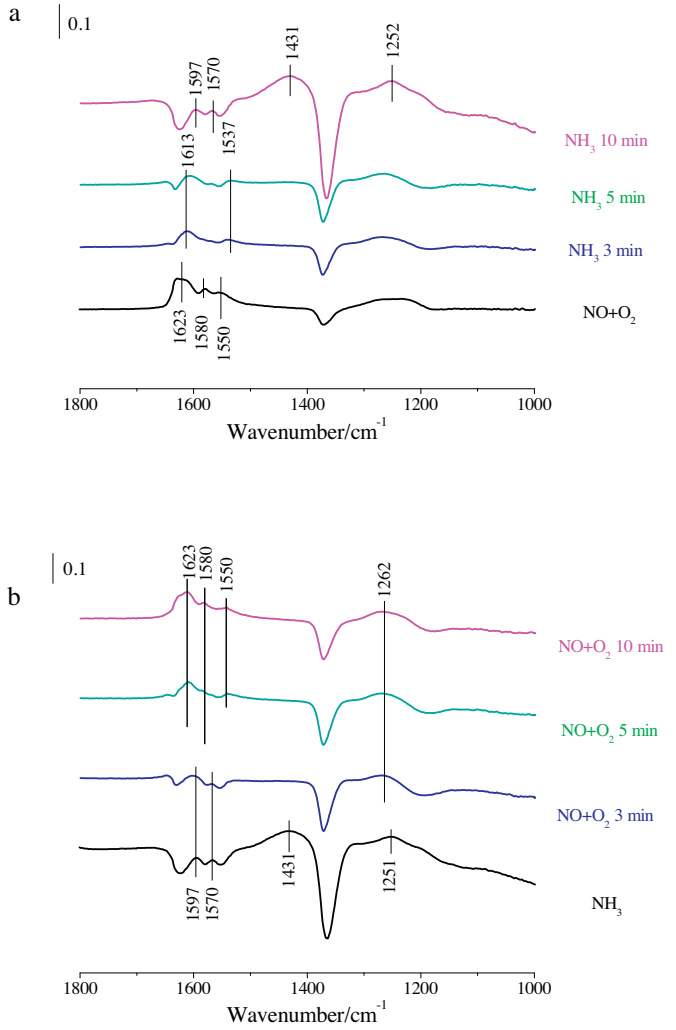

Fig. 9. (a), In situ DRIFT spectra taken at 150 °C upon passing NH_3 over $NO + O_2$ presorbed 10% Mn/Fe–Ti spinel; (b), In situ DRIFT spectra taken at 150 °C upon passing $NO + O_2$ over NH_3 presorbed 10% Mn/Fe–Ti spinel.

$$NH_{3(ad)} + M^{(n-1)+}\text{—O—NO} \rightarrow M^{(n-1)+}\text{—O—NO—}NH_3 \rightarrow Mn^{(n-1)+}\text{—OH} + N_2 + H_2O \quad (5)$$

$$Mn^{(n-1)+}\text{- O- }NO_2 + NH_{3(ad)} \rightarrow M^{(n-1)+}\text{- O- }NO_2\text{- }NH_3 \rightarrow M^{(n-1)+}\text{- OH} + N_2O + H_2O \quad (6)$$

$$M^{(n-1)+}\text{- OH} + \frac{1}{4}O_2 \rightarrow M^{n+} = O + \frac{1}{2}H_2O \quad (7)$$

Reactions (1) and (2) were the adsorption of gaseous NH_3 and NO on the surface, respectively. There is generally agreement the SCR reaction starts with the adsorption of gaseous NH_3 [1,28]. Physically adsorbed NO can be oxidized by M^{n+} (i.e., Fe^{3+} and/or Mn^{4+} on Fe–Ti spinel, 10% Fe–Ti spinel and 5% Mn–10% Fe/TiO_2) to form monodentate nitrite and monodentate nitrate (i.e., Reactions (3) and (4)). Then, adsorbed monodentate nitrite and monodentate nitrate reacted with adsorbed NH_3 to form NH_4NO_2 and NH_4NO_3 (i.e., Reactions (5) and (6)), which were then decomposed to N_2 and N_2O respectively. The reduced M^{n+} can be rapidly regenerated by the reaction with gaseous O_2 (i.e. Reaction (7)).

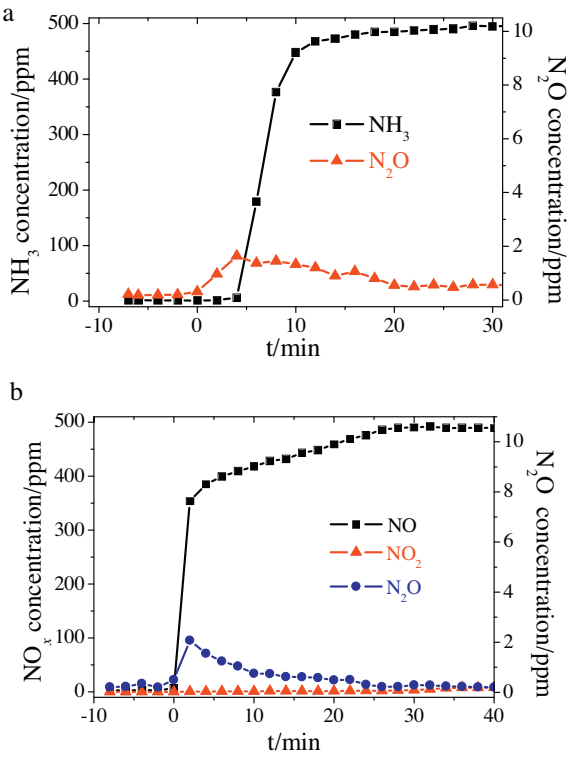

Fig. 10. (a), NH_3 and N_2O concentrations in the outlet during passing NH_3 over $NO + O_2$ presorbed 10% Mn/Fe–Ti spinel at 150 °C; (b), NO_x and N_2O concentrations in the outlet during passing $NO + O_2$ over NH_3 presorbed 10% Mn/Fe–Ti spinel at 150 °C.

NO reduction through the Eley–Rideal mechanism can be approximately described as [1,14,29,30]:

$$NH_{3(g)} \rightarrow NH_{3(ad)} \quad (1)$$

$$NH_{3(ad)} + M^{n+} = O \rightarrow NH_2 + M^{(n-1)+} - OH \quad (8)$$

$$NH_2 + M^{n+} = O \rightarrow NH + M^{(n-1)+}\text{- OH} \quad (9)$$

$$NH_2 + NO_{(g)} \rightarrow N_2 + H_2O \quad (10)$$

$$NH + NO_{(g)} \rightarrow N_2O + H^+ \quad (11)$$

Adsorbed NH_3 can be activated by M^{n+} (including Mn^{4+} and Fe^{3+}) on the surface to NH_2 (i.e., Reaction (8)). Meanwhile, NH_2 on the surface can be further oxidized to NH by M^{n+} on the surface (i.e., Reaction (9)). There is generally agreement that the reaction products of gaseous NO with NH_2 and NH (i.e., Reactions (10) and (11)) were N_2 and N_2O, respectively [1]. A lot of N_2O formed during NO reduction over Mn based low temperature SCR catalyst, while little N_2O formed during NO reduction over Fe based SCR catalyst. It suggests NH_2 on the surface cannot be oxidized to NH by Fe^{3+} and the oxidation of NH_2 on 5% Mn–10% Fe/TiO_2 and 10% Mn/Fe–Ti spinel to NH was mainly related to Mn^{4+} on the surface.

4.2. Steady state kinetic study

The kinetic equations of N_2 and N_2O formation through the Langmuir–Hinshelwood mechanism can be approximately described as:

$$\frac{d[N_2]}{dt}|_{L-H} = k_1[M^{(n-1)+}\text{- O- NO- }NH_3] \quad (12)$$

$$\frac{d[N_2O]}{dt}|_{L-H} = k_2[M^{(n-1)+}\text{- O- }NO_2\text{- }NH_3] \quad (13)$$

where, k_1, k_2, $[M^{(n-1)+}\text{—O—NO—NH}_3]$, and $[M^{(n-1)+}\text{—O—NO}_2\text{–NH}_3]$ were the decomposition rate constants of NH_4NO_2 and NH_4NO_3, and the concentrations of NH_4NO_2 and NH_4NO_3 on the surface, respectively.

The kinetic equations of NH_4NO_2 and NH_4NO_3 formation (i.e., Reactions (5) and (6)) can be approximately described as:

$$\frac{d[M^{(n-1)+}\text{- O- NO- NH}_3]}{dt} = k_3[M^{(n-1)+}\text{- O- NO}]\left[NH_{3(ad)}\right] \quad (14)$$

$$\frac{d[M^{(n-1)+}\text{- O- NO}_2\text{- NH}_3]}{dt} = k_4[M^{(n-1)+}\text{- O- NO}_2]\left[NH_{3(ad)}\right] \quad (15)$$

where, k_3, k_4, $[M^{(n-1)+}\text{—O—NO}]$, $[M^{(n-1)+}\text{—O—NO}_2]$ and $[NH_{3(ad)}]$ were the reaction kinetic constants of Reactions (5) and (6), and the concentrations of monodentate nitrite, monodentate nitrate and NH_3 adsorbed on the surface, respectively.

The kinetic equations of monodentate nitrite and monodentate nitrate formation (i.e., Reactions (3) and (4)) can be approximately described as:

$$\frac{d[M^{(n-1)+}\text{- O- NO}]}{dt} = k_5[M^{n+}=O][NO_{(ad)}] \quad (16)$$

$$\frac{d[M^{(n-1)+}\text{- O- NO}_2]}{dt} = k_6[M^{n+}=O][NO_{(ad)}][O_2]^{\frac{1}{2}} \quad (17)$$

where, k_5, k_6, $[M^{n+}=O]$ and $[NO_{(ad)}]$ were the reaction kinetic constants of Reactions (3) and (4), and the concentrations of M^{n+} and NO adsorbed on the surface, respectively.

As the GHSV used was quite high, the conversions of NH_3 and NO were very low. Therefore, there were large amounts of NO_x and NH_3 in the outlet. The SCR catalyst was almost saturated with the adsorption of gaseous NO and NH_3, so the concentrations of NO adsorbed and NH_3 adsorbed (i.e., $[NO_{(ad)}]$ and $[NH_{3(ad)}]$) on the SCR catalyst can be approximately regarded as constants, which were not related to the concentrations of gaseous NO and NH_3 [14,21]. Meanwhile, the concentration of M^{n+} on the surface can be regarded as a constant at the steady state as it can be rapidly recovered through Reaction (7). Hinted by Eqs. (14)–(17), the formation of NH_4NO_2 and NH_4NO_3 (i.e., the concentrations of NH_4NO_2 and NH_4NO_3 on the surface) were both approximately not related to the concentrations of gaseous NO and NH_3. Hinted by Eqs. (12) and (13), the formations of N_2 and N_2O through the Langmuir–Hinshelwood mechanism were approximately independent of gaseous NO concentration. This result was widely demonstrated on MnO_x-CeO_2 and Mn–Fe spinel [15,19,26,31].

The kinetic equations of N_2 and N_2O formation through the Eley–Rideal mechanism (i.e., Reactions (10) and (11)) can be described as:

$$\frac{d[N_2]}{dt}|_{E-R} = -\frac{d[NO_{(g)}]}{dt} = k_7[NH_2][NO_{(g)}] \quad (18)$$

$$\frac{d[N_2O]}{dt}|_{E-R} = -\frac{d[NO_{(g)}]}{dt} = -\frac{d[NH]}{dt} = k_8[NH][NO_{(g)}] \quad (19)$$

where, k_7, k_8, $[NH_2]$, [NH] and $[NO_{(g)}]$ were the reaction rate constants of Reactions (10) and (11), the concentrations of NH_2 and NH on the surface, and gaseous NO concentration, respectively.

The reaction kinetic equations of NH_2 and NH formation on the surface (i.e., Reactions (8) and (9)) can be described as:

$$\frac{d[NH_2]}{dt} = k_9\left[NH_{3(ad)}\right][M^{n+}=O] \quad (20)$$

$$\frac{d[NH]}{dt} = k_{10}[NH_2][Mn^{4+}=O] \quad (21)$$

where, k_9, k_{10}, $[M^{n+}=O]$ and $[Mn^{4+}=O]$ were the reaction kinetic constant of Reactions (8) and (9), and the concentrations of M^{n+} and Mn^{4+} on the surface respectively.

According to Eqs. (19) and (21), the variation of NH concentration can be described as:

$$\frac{d[NH]}{dt} = k_{10}[NH_2][Mn^{4+}=O] - k_8[NH][NO_{(g)}] \quad (22)$$

As the reaction reached the steady state, NH concentration did not vary. Therefore,

$$\frac{d[NH]}{dt} = k_{10}[NH_2][Mn^{4+}=O] - k_8[NH][NO_{(g)}] = 0 \quad (23)$$

Hence,

$$[NH] = \frac{k_{10}[NH_2][Mn^{4+}=O]}{k_8[NO]} \quad (24)$$

Then, N_2O formation through the Eley–Rideal mechanism (i.e., Eq. (19)) can be described as:

$$\frac{d[N_2O]}{dt}|_{E-R} = k_8\frac{k_{10}[NH_2][Mn^{4+}=O]}{k_8[NO_{(g)}]}[NO_{(g)}] = k_{10}[NH_2][Mn^{4+}=O] \quad (25)$$

Our previous study demonstrated that NH_2 on the surface was independent of the concentrations of gaseous NO and NH_3 at the steady state [15,26], which was mainly related to k_9, the concentrations of NH_3 adsorbed and M^{n+} on the surface (hinted by Eq. (20)).Taking account of the contributions of both the Eley–Rideal mechanism and the Langmuir–Hinshelwood mechanism, the kinetic equations of NO reduction and N_2O formation can be approximately described as:

$$\begin{aligned} k_{NO} &= -\frac{d[NO_{(g)}]}{dt} = -\frac{d[NO_{(g)}]}{dt}|_{E-R} - \frac{d[NO_{(g)}]}{dt}|_{L-H} = k_7[NH_2][NO_{(g)}] \\ &+k_{10}[NH_2][Mn^{4+}=O]+k_1[M^{(n-1)+}\text{- O- NO- NH}_3]+k_2[M^{(n-1)+}\text{- O- NO}_2\text{- NH}_3] \\ &= k_{SCR-ER}[NO_{(g)}] + k_{SCR-LH} + k_{NSCR} \end{aligned} \quad (26)$$

$$\begin{aligned} k_{NSCR} &= \frac{d[N_2O]}{dt} = \frac{d[N_2O]}{dt}|_{E-R} + \frac{d[N_2O]}{dt}|_{L-H} \\ &= k_{10}[NH_2][Mn^{4+}=O]+k_2[M^{(n-1)+}\text{- O- NO}_2\text{- NH}_3] \end{aligned} \quad (27)$$

$$k_{SCR-ER} = k_7[NH_2] \quad (28)$$

$$k_{SCR-LH} = k_1[M^{(n-1)+}\text{- O- NO- NH}_3] \quad (29)$$

where, k_{NO}, k_{SCR-ER}, k_{SCR-LH} and k_{NCR} were the rate of NO reduction, the reaction rate constant of the SCR reaction (i.e. N_2 formation) through the Eley–Rideal mechanism, the reaction rate constant of the SCR reaction through the Langmuir–Hinshelwood mechanism, and the reaction rate constant of the NSCR reaction (i.e., N_2O formation), respectively.

To obtain these reaction kinetic constants, the steady-state kinetic study was performed. As shown in Fig. 11, there was an excellent linear relationship between the rate of NO reduction and gaseous NO concentration, which was consistent with the hint of Eq. (26). Meanwhile, the rate of N_2O formation hardly varied after the increase of gaseous NO concentration (shown in Fig. 12). It suggests that the rate of N_2O formation was approximately independent of gaseous NO concentration, which was consistent with the hint of Eq. (27). Therefore, k_{NSCR} can be directly obtained through Fig. 12. Hinted by Eq. (26), k_{SCR-ER} and k_{SCR-LH} can be obtained after the linear regression of Fig. 11 (the slope was k_{SCR-ER} and the intercept was the sum of k_{SCR-LH} and k_{NSCR}).

As shown in Table 3, both k_{SCR-ER} and k_{SCR-LH} of Fe–Ti spinel increased after the load of MnO_x. It suggests that the SCR reaction over Fe–Ti spinel through both the Eley–Rideal mechanism and the Langmuir–Hinshelwood mechanism were promoted after the load of MnO_x. Although k_{NSCR} of Fe–Ti spinel slightly increased after the load of MnO_x, k_{NSCR} of 10% Mn/Fe–Ti spinel was much less than that

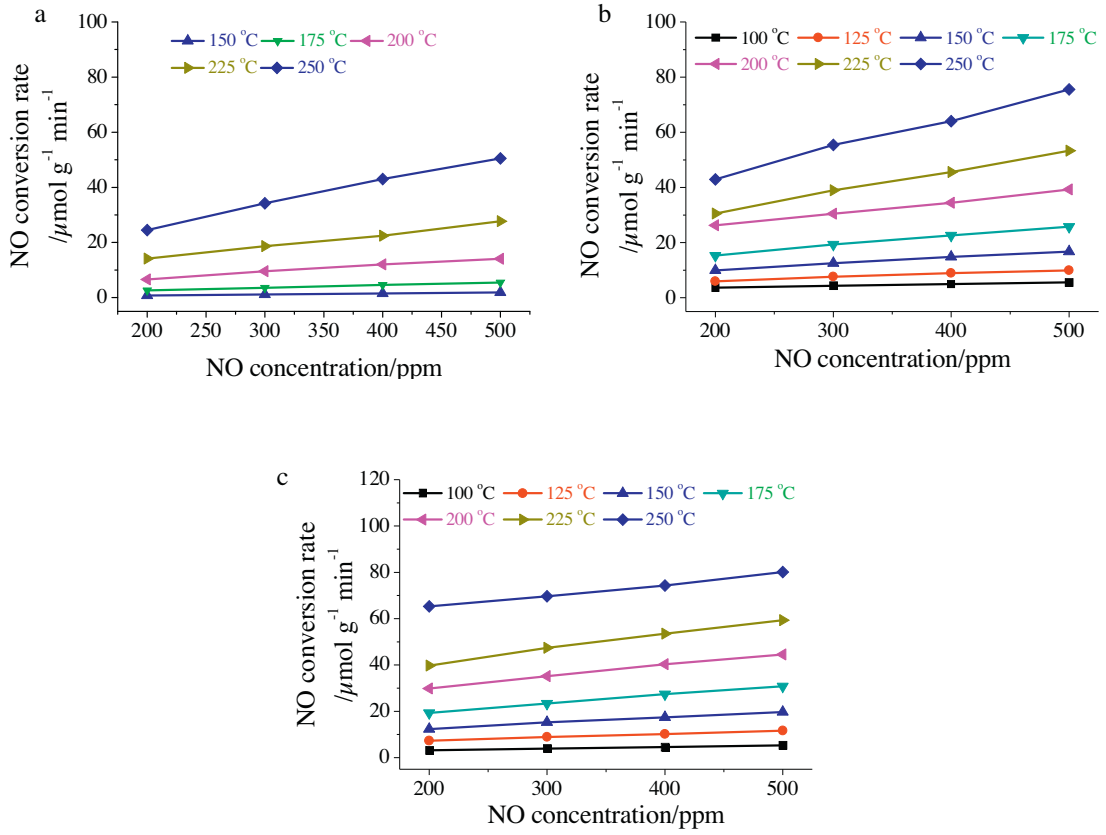

Fig. 11. Dependences of NO conversion rate on gaseous NO concentration during the SCR reaction over: (a), Fe–Ti spinel; (b), 10% Mn/Fe-Ti spinel; (c), 5% Mn-10% Fe/TiO_2. Reaction conditions: [NH_3] = 500 ppm, [NO] = 200–500 ppm, [O_2] = 2%, catalyst mass = 5–100 mg, total flow rate = 200 mL min^{-1} and GHSV = 120000–2400000 cm^3 g^{-1} h^{-1}.

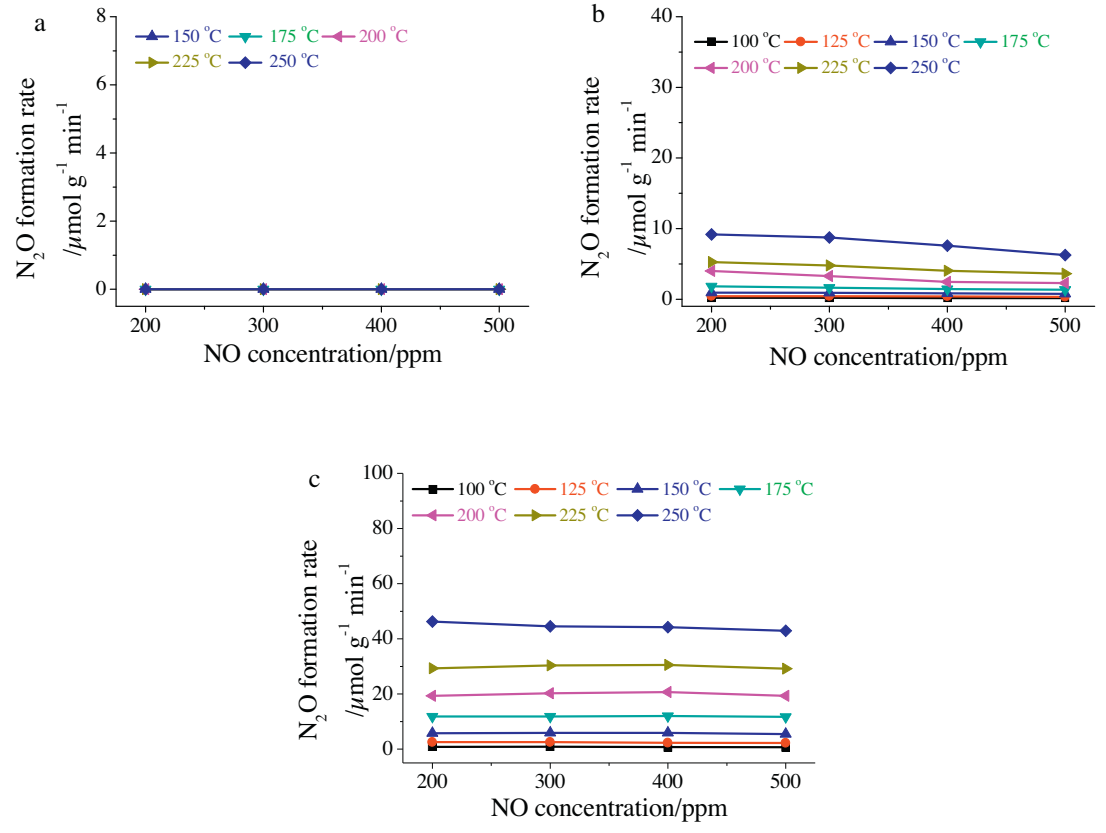

Fig. 12. Dependences of N_2O formation rate on gaseous NO concentration during the SCR reaction over: (a), Fe–Ti spinel; (b), 10% Mn/Fe–Ti spinel; (c), 5% Mn–10% Fe/TiO_2. Reaction conditions: [NH_3] = 500 ppm, [NO] = 200–500 ppm, [O_2] = 2%, catalyst mass = 5–100 mg, total flow rate = 200 mL min^{-1} and GHSV = 120000–2400000 cm^3 g^{-1} h^{-1}.

Table 3
The rate constants of the SCR reaction through the Eley–Rideal mechanism ($k_{SCR\text{-}ER}$), the rate constants of the SCR reaction through the Langmuir–Hinshelwood mechanism ($k_{SCR\text{-}LH}$), and the rate constants of the NSCR reaction (k_{NSCR}) /μmol g^{-1} min^{-1}.

Temperature/°C		$k_{NO} = k_{SCR\text{-}ER}[NO_{(g)}] + k_{SCR\text{-}LH} + k_{NSCR}$			R^2	k_{NO}	k_{SCR}
		$k_{SCR\text{-}LH}$	$k_{SCR\text{-}ER}/10^6$	k_{NSCR}		[NH$_3$] = [NO]	=500 ppm
5%Mn–10% Fe/TiO$_2$	100	1.0	0.0071	0.8	0.999	5.3	4.5
	125	2.1	0.014	2.4	0.998	11.5	9.1
	150	1.9	0.024	5.8	0.995	19.7	13.9
	175	0	0.039	11.8	0.998	30.8	19.0
	200	0.4	0.049	19.9	0.997	44.5	24.6
	225	0	0.065	29.2	0.996	59.3	30.1
	250	10.7	0.049	44.5	0.995	80.1	35.6
Fe-Ti spinel	150	0.045	0.0036	0	0.999	1.9	1.9
	175	0.74	0.0095	0	0.998	5.4	5.4
	200	1.8	0.025	0	0.992	14.1	14.1
	225	5.2	0.045	0	0.996	27.7	27.7
	250	7.0	0.087	0	0.997	50.5	50.5
10%Mn/Fe–Ti spinel	100	2.2	0.0063	0.2	0.999	5.6	5.4
	125	3.1	0.013	0.4	0.986	9.9	9.5
	150	4.7	0.023	0.9	0.996	16.7	15.8
	175	7.0	0.035	1.6	0.997	25.8	24.2
	200	14.6	0.043	3.0	0.998	39.3	36.3
	225	13.7	0.070	4.4	0.998	53.3	48.9
	250	14.3	0.11	7.9	0.996	75.5	67.6

of 5% Mn–10% Fe/TiO$_2$. Table 3 also shows that k_{SCR} of 10% Mn/Fe–Ti spinel was much more than that of 5% Mn–10% Fe/TiO$_2$. As a result, N_2O selectivity of NO reduction over 10% Mn/Fe–Ti spinel was much less than that over 5% Mn–10% Fe/TiO$_2$ (shown in Fig. 3a).

In our previous study, the parameters of $k_{SCR\text{-}ER}$ and k_{NSCR} of Mn–Fe spinel were reported [19]. Although $k_{SCR\text{-}ER}$ of 10% Mn/Fe–Ti spinel was approximately 20% of that of Mn–Fe spinel at 200 °C, k_{NSCR} of 10% Mn/Fe–Ti spinel was only approximately 4% of that of Mn–Fe spinel. As a result, N_2 selectivity of 10% Mn/Fe–Ti spinel was much better than that of Mn–Fe spinel.

4.3. Mechanism of the load of MnO_x on NO reduction over Fe–Ti spinel

As shown in Table 2, the adsorption of NO on Fe–Ti spinel was promoted after the load of MnO_x. It suggests that [$NO_{(ad)}$] on 10% Mn/Fe–Ti spinel was much higher than that on Fe–Ti spinel. As is well known, the oxidation ability of Mn^{4+} is much high than that of Fe^{3+} (hinted by Fig. 4). It suggests that k_5 and k_6 of 10% Mn/Fe–Ti spinel were much higher than those of Fe–Ti spinel. Hinted by Eqs. (16) and (17), the adsorption of NO_x over Fe–Ti spinel were promoted after the load of MnO_x and the concentrations of monodentate nitrite and monodentate nitrate on 10% Mn/Fe–Ti spinel were much higher than those over Fe–Ti spinel. Hinted by Eqs. (12)–(17), both $k_{SCR\text{-}LH}$ and k_2[$M^{(n-1)+}$—O—NO_2—NH_3] of 10% Mn/Fe–Ti spinel were much higher than those of Fe–Ti spinel (shown in Table 3). Therefore, both N_2 and N_2O formation over Fe–Ti spinel through the Langmuir–Hinshelwood mechanism were promoted after the load of MnO_x.

Fig. 7 demonstrated that N_2O formation over 5% Mn–10% Fe/TiO$_2$ mainly resulted from the Eley–Rideal mechanism (i.e., the reaction of NH with gaseous NO). It suggests that a large amount of NH_2 on 5% Mn–10% Fe/TiO$_2$ was oxidized to NH by Mn^{4+} on the surface. However, only a small amount of N_2O resulted from NO reduction over 10% Mn/Fe–Ti spinel through the Eley–Rideal mechanism (shown in Fig. 10b). It suggests that NH_2 on 10% Mn/Fe–Ti spinel can hardly be oxidized to NH although the concentration of Mn^{4+} on 10% Mn/Fe–Ti spinel was much higher than that on 5% Mn–10% Fe/TiO$_2$ (shown in Table 1).

In situ DRIFTS study demonstrated that the acid sites on 10% Mn/Fe–Ti spinel mainly resulted from the support (i.e. Fe–Ti spinel), so NH_3/NH_2 mainly adsorbed on the support of 10% Mn/Fe–Ti spinel, which was far away from Mn^{4+} cations on 10% Mn/Fe–Ti spinel. Therefore, NH_2 on 10% Mn/Fe–Ti spinel can hardly be oxidized by Mn^{4+} on the surface to NH. As a result, only a small amount of N_2O formed over 10% Mn/Fe–Ti spinel through the Eley–Rideal mechanism (shown in Fig. 10b).

The resistivity of Fe–Ti spinel is lower and its conductivity is almost metallic, which are similar to those of magnetite [32]. Therefore, the electron can migrate easily between the bulk and the surface. The redox potential of the oxidation of Fe^{2+} by Mn^{4+} is 0.18 V, so Reaction (30) is thermodynamically favorable. They suggest that the regeneration of Fe^{3+} on Fe–Ti spinel can be accelerated after the load of MnO_x. Therefore, the activation of adsorbed NH_3 to NH_2 over Fe–Ti spinel was promoted after the load of MnO_x resulting in a higher concentration of NH_2 on 10% Mn/Fe–Ti spinel although NH_3 adsorbed on 10% Mn/Fe-Ti spinel cannot be directly activated by Mn^{4+} on 10% Mn/Fe–Ti spinel. Hinted by Eq. (28), $k_{SCR\text{-}ER}$ of 10% Mn/Fe–Ti spinel was much higher than that of Fe–Ti spinel (shown in Table 3). As a result, the SCR reaction over Fe–Ti spinel through the Eley–Rideal mechanism was remarkably promoted after the load of MnO_x.

$$\equiv Fe^{2+} + \equiv Mn^{4+} \rightarrow \equiv Fe^{3+} + \equiv Mn^{3+} \quad E^0 = 0.18\ eV \tag{30}$$

5. Conclusion

10% Mn/Fe–Ti spinel showed an excellent SCR performance including SCR activity and N_2 selectivity at low temperatures, which was much better than 5% Mn–10% Fe/TiO$_2$ with the same chemical composition. As NH_3 and NH_2 were mainly adsorbed on the support of 10% Mn/Fe–Ti spinel, they were far away from Mn^{4+} on 10% Mn/Fe–Ti spinel. Therefore, the over-activation of adsorbed NH_2 to NH by Mn^{4+} can hardly happen on 10% Mn/Fe–Ti spinel resulting in a suppression of N_2O formation through the Eley–Rideal mechanism. However, the regeneration of Fe^{3+} on Fe–Ti spinel was accelerated after the load of MnO_x due to the rapid electron transfer between Mn^{4+} and Fe^{2+} on 10% Mn/Fe–Ti spinel, resulting in a remarkable promotion on NH_3 activation. Therefore, the SCR reaction over Fe–Ti spinel was remarkably promoted after the load of MnO_x although Mn^{4+} did not take part in the activation of adsorbed NH_3.

Acknowledgements

This study was financially supported by the National Natural Science Fund of China (Grant no. 21207067, 41372044 and 21325731), the Priority Academic Program Development of Jiangsu Higher Education Institutions, the Zijin Intelligent Program, Nanjing University of Science and Technology (Grant No. 2013-0106) and ITSP Tier 3 Scheme (ITS/273/13) by Innovation Technology Commission, Hong Kong SAR Government.

Appendix A. Supplementary data

Supplementary data associated with this article can be found, in the online version, at http://dx.doi.org/10.1016/j.apcatb.2015.08.023.

References

[1] G. Busca, L. Lietti, G. Ramis, F. Berti, Appl. Catal. B-Environ. 18 (1998) 1–36.
[2] N.Y. Topsoe, Science 265 (1994) 1217–1219.
[3] C. Wang, S. Yang, H. Chang, Y. Peng, J. Li, Chem. Eng. J. 225 (2013) 520–527.
[4] Y. Liu, T.T. Gu, X.L. Weng, Y. Wang, Z.B. Wu, H.Q. Wang, J. Phys. Chem. C 116 (2012) 16582–16592.
[5] G.S. Qi, R.T. Yang, J. Catal. 217 (2003) 434–441.
[6] M. Wallin, S. Forser, P. Thormahlen, M. Skoglundh, Ind. Eng. Chem. Res. 43 (2004) 7723–7731.
[7] Y.J. Kim, H.J. Kwon, I.S. Nam, J.W. Choung, J.K. Kil, H.J. Kim, M.S. Cha, G.K. Yeo, Catal. Today 151 (2010) 244–250.
[8] G.S. Qi, R.T. Yang, Appl. Catal. B-Environ. 44 (2003) 217–225.
[9] M. Casapu, O. Krocher, M. Elsener, Appl. Catal. B-Environ. 88 (2009) 413–419.
[10] G.S. Qi, R.T. Yang, R. Chang, Appl. Catal. B-Environ. 51 (2004) 93–106.
[11] R.B. Jin, Y. Liu, Y. Wang, W.L. Cen, Z.B. Wu, H.Q. Wang, X.L. Weng, Appl. Catal. B-Environ. 148 (2014) 582–588.
[12] Z.M. Liu, J.Z. Zhu, J.H. Li, L.L. Ma, S.I. Woo, ACS Appl. Mater. Interface 6 (2014) 14500–14508.
[13] Z.M. Liu, Y. Li, T.L. Zhu, H. Su, J.Z. Zhu, Ind. Eng. Chem. Res. 53 (2014) 12964–12970.
[14] S. Yang, C. Wang, J. Li, N. Yan, L. Ma, H. Chang, Appl. Catal. B-Environ. 110 (2011) 71–80.
[15] S. Yang, S. Xiong, Y. Liao, X. Xiao, F. Qi, Y. Peng, Y. Fu, W. Shan, J. Li, Environ. Sci. Technol. 48 (2014) 10354–10362.
[16] D.E. Canfield, A.N. Glazer, P.G. Falkowski, Science 330 (2010) 192–196.
[17] M.J. Prather, J. Hsu, Science 330 (2010) 952–954.
[18] A.R. Ravishankara, J.S. Daniel, R.W. Portmann, Science 326 (2009) 123–125.
[19] S. Xiong, Y. Liao, X. Xiao, H. Dang, S. Yang, Catal. Sci. Technol. 5 (2015) 2132–2140.
[20] S. Yang, Y. Guo, N. Yan, D. Wu, H. He, Z. Qu, C. Yang, Q. Zhou, J. Jia, ACS Appl. Mater. Interface 3 (2011) 209–217.
[21] S.J. Yang, J.H. Li, C.Z. Wang, J.H. Chen, L. Ma, H.Z. Chang, L. Chen, Y. Peng, N.Q. Yan, Appl. Catal. B-Environ. 117 (2012) 73–80.
[22] S. Yang, F. Qi, Y. Liao, S. Xiong, Y. Lan, Y. Fu, W. Shan, J. Li, Ind. Eng. Chem. Res. 53 (2014) 5810–5819.
[23] G.S. Qi, R.T. Yang, J. Phys. Chem. B 108 (2004) 15738–15747.
[24] B.Q. Jiang, Z.B. Wu, Y. Liu, S.C. Lee, W.K. Ho, J. Phys. Chem. C 114 (2010) 4961–4965.
[25] K.I. Hadjiivanov, Catal. Rev. 42 (2000) 71–144.
[26] S. Yang, Y. Liao, S. Xiong, F. Qi, H. Dang, X. Xiao, J. Li, J. Phys. Chem. C 118 (2014) 21500–21508.
[27] G.S. Qi, R.T. Yang, Chem. Commun. 7 (2003) 848–849.
[28] M. Machida, M. Uto, D. Kurogi, T. Kijima, J. Mater. Chem. 11 (2001) 900–904.
[29] S. Yang, Y. Fu, Y. Liao, S. Xiong, Z. Qu, N. Yan, J. Li, Catal. Sci. Technol. 4 (2014) 224–232.
[30] X.F. Tang, J.H. Li, L.A. Sun, J.M. Hao, Appl. Catal. B-Environ. 99 (2010) 156–162.
[31] S. Xiong, Y. Liao, X. Xiao, H. Dang, S. Yang, J. Phys. Chem. C 119 (2015) 4180–4187.
[32] S.J. Yang, C.Z. Wang, L. Ma, Y. Peng, Z. Qu, N.Q. Yan, J.H. Chen, H.Z. Chang, J.H. Li, Catal. Sci.Technol. 3 (2013) 161–168.